High-temperature phase transition in the three-layered sodium cobaltite $P'3$-Na_xCoO_2 ($x \sim 0.62$)

Maxime Blangero,* Dany Carlier, Michaël Pollet, Jacques Darriet, Claude Delmas, and Jean-Pierre Doumerc
ICMCB, CNRS, Université Bordeaux 1, 87 Av. du Dr. A. Schweitzer, 33608 Pessac Cedex, France
(Received 2 October 2007; revised manuscript received 7 April 2008; published 21 May 2008)

The high temperature phase transition in the three-layered $P'3$-Na_xCoO_2 ($x \sim 0.62$) has been investigated by means of heat capacity measurement, x-ray diffraction, and ^{23}Na magic angle spinning (MAS)–NMR spectroscopy in the 300–550 K range. The phase transition occurs nearby $T_S = 350$ K. Below T_S, the unit cell is monoclinic (space group $C2/m$). Above T_S, the monoclinic cell is reversibly converted into a rhombohedral cell (space group $R3m$). The crystallographic change mainly manifests into Na rearrangement in the interslab from a low symmetry position to a higher symmetry position. A global picture for both systems of the (x,y,z) off-center position of Na could be understood as a balance between on-site Na^+-$Co^{3+/4+}$ electrostatic repulsions (z shift) and in-plane Na^+-Na^+ electrostatic repulsions (xy shift). We suggest that Na^+ interlayer redistribution is the driving force of the phase transition. ^{23}Na MAS-NMR spectroscopy has been used to investigate changes in the environment and in the distribution of the sodium cations occurring by raising the temperature. The gradual suppression of the second-order quadrupolar interactions and the resulting new resonance is consistent with the sodium site exchange mechanism. Changes in the resistivity at T_S suggest a strong coupling between the Na^+ and CoO_2 layers.

DOI: 10.1103/PhysRevB.77.184116 PACS number(s): 68.18.Jk, 61.05.cp, 61.72.Hh, 65.40.Ba

I. INTRODUCTION

In the 1980s, Na_xCoO_2 has been widely investigated as potential electrode materials for sodium batteries in Bordeaux.[1] The same research group reported the thermodynamic phase diagram of Na_xCoO_2 and measured the unusually large thermoelectric power of 80 $\mu V/K$ associated with low metallicklike electrical resistivity of 3 $m\Omega$ cm at 300 K for polycrystalline $Na_{0.7}CoO_2$ powder.[2,3] More recently, Na_xCoO_2 gained a renewed interest after the measurement of the promising thermoelectric power factor of $Na_{\sim 0.7}CoO_2$ single crystals[4] and the discovery of superconductivity in hydrated $Na_{0.35}CoO_2\ 1.3H_2O$.[5]

Four thermodynamic stable phase domains have been identified depending on the alkali content.[6] All phases consist of an alternate stacking of slabs of edge-shared CoO_6 octahedra and of partially deficient alkali layers. They differ in the packing sequence of oxygen layers that leads to different oxygen environments for Na^+ ions, octahedral (O), or prismatic (P) and to a different number of CoO_2 sheets—2 or 3—within the pseudohexagonal unit cell. According to Fouassier *et al.*[7] nomenclature, three of them are three-layered structures and are designated by O3 for $0.9 \leq x \leq 1$, $O'3$ for $x = 0.75$, and $P'3$ for $0.55 \leq x \leq 0.68$; the prime superscript refers to a monoclinic distortion of the unit cell. Only for $x \sim 0.7$ a two-layered $P2$ structure with interesting thermoelectric properties is obtained.

In $P'3$-Na_xCoO_2, all the Na^+ ions are occupying a single type of prismatic site that on one side is sharing a face and on the other side is sharing edges with surrounding CoO_6 octahedra. This situation is very different from that of $P2$-Na_xCoO_2, where two distinct prismatic sites are found: one is sharing only faces, whereas the second one is sharing only edges with CoO_6 octahedra. The room temperature monoclinic distortion β of the $P'3$ family has been accurately determined.[8,9] The monoclinic unit cell contains a single layer and the space group is $C2/m$. For $x = 0.6$,[9] the monoclinic angle β is equal to 106.05°, which is slightly less than the corresponding angle of 106.52° deduced from the pseudohexagonal cell reported by Fouassier *et al.*[6]

The physical properties of this system in the low temperature region have been widely investigated. Little is, however, known about the high temperature behavior of this oxide family. In this study, a high temperature phase transition from a monoclinic to a higher rhombohedral symmetry is reported and its temperature dependence is followed by means of x-ray diffraction (XRD) and ^{23}Na magic angle spinning (MAS)–NMR. Other groups studied the $P2$ compounds as single crystal or aligned powder with broad line-type NMR spectrometers. In these studies, Na^+ ions are said to be mobile from ~200 K to 250 K.[10,11] However, we show by variable temperature ^{23}Na MAS-NMR that Na^+ ions are not fully exchanged at room temperature and that the motion is activated upon heating. Anomalies in the temperature dependences of the specific heat and electrical resistivities are discussed regarding this phase transition.

II. EXPERIMENT

The synthesis of polycrystalline powder of $P'3$-Na_xCoO_2 ($x \approx 0.62$) has already been reported in detail.[6] In short, a conventional solid-state reaction route has been used: Powders of Na_2O and Co_3O_4 were intimately mixed under argon in a glovebox and heated for 12 h to 823 K under dry oxygen flow. Since by-produced Na_2O is highly volatile, a 10 wt % excess is added. After heating and cooling, the black product was immediately put under dry argon atmosphere to prevent moisture contamination. All the characterizations were performed on the same batch.

XRD patterns of $Na_{0.62}CoO_2$ were recorded with a Philips X'Pert Pro powder diffractometer in the Bragg–Brentano geometry by using Co $K\alpha$ radiations. The data collections were

made in the 10° – 120° 2θ range with a 0.0167° step by using an X'Celerator PSD detector. The powder was kept in an airtight holder under dry argon for room temperature x-ray diffraction to prevent any reaction with air moisture (linear PSD aperture of 0.512 mm and counting time of 240 s/step). High temperature x-ray diffraction was performed in an Anton Paar HTK 1200N oven chamber under dry oxygen flow (linear PSD aperture of 1.019 mm and counting time of 350 s/step).

The diffraction data were analyzed by using the Rietveld technique,[12] as implemented in the FULLPROF program.[13] The peak shape was described by a pseudo-Voigt function, and the background level was fitted with linear interpolation between a set of given points with refinable heights. The sodium content of the unit cell was set according to inductively coupled plasma–atomic emission spectrometry elementary determination that leads to the raw formula $Na_{0.62(2)}CoO_2$.

Single pulse ^{23}Na MAS-NMR spectra were recorded on a Bruker 300 Avance spectrometer at 79.403 MHz with a standard 4 mm Bruker MAS probe. Polycrystalline samples were mixed with dry silica (typically in a 1:1 weight ratio) in order to facilitate the spinning and improve the field homogeneity since they may exhibit metallic or paramagnetic properties. The mixture was placed in 4 mm diameter zirconia rotors in a dry box. No change in the NMR signal was observed even for rotors that were kept several days out of the dry box, indicating good air tightness of the cell. A short pulse length of 1 μs corresponding to a selective $\pi/12$ pulse determined by using an aqueous 0.1 mol/l NaCl solution was employed. A spinning speed of 13 kHz was used. The spectral width was set to 1 MHz, and the recycle time, $D_0=0.5$ s, was long enough to avoid T_1 saturation effects with 1600 scans per spectrum. The base line distortions resulting from the spectrometer dead time (5–10 μs) were computationally removed by using a polynomial base line correction routine. 1600 scans variable temperature NMR experiments were also carried out in the 300–470 K range by using a Bruker WVT MAS probe. The external reference was a 0.1 mol/l NaCl aqueous solution.

Heat capacity measurements were made in a helium Quantum Design PPMS cryostat using the "2τ relaxation method" in the 1.8–400 K range under high vacuum. Above 300 K, sample radiation losses may affect the specific heat accuracy. The sample heat capacity is calculated by carefully subtracting a blank measurement, including both the contributions of the sample platform and of the grease used to attach the sample to the puck, from the total heat capacity measurement. C_p for C_v correction has not been performed as the resulting error is assumed negligible in the explored temperature range (around 5% for $T\sim\theta_D$).

Field cooled dc-magnetization data in an applied field of 1 T were collected on a superconducting quantum interference device magnetometer (Quantum Design) in the 2–300 K temperature range. For higher temperature ranges (i.e., 300–500 K), the paramagnetic susceptibility was measured on a DSM-8 stationary pendulum susceptometer of Manics Équipement Scientifique under an applied field of 1 T. Field dependency of the magnetization was found linear down to 5 K. Transport properties were measured on raw pellets (10 mm in diameter) pressed under 10 MPa, the compactness of which was close to 70%. Electrical dc conductivity measurements were performed with the aligned four-probe method in the 4.2–500 K range.

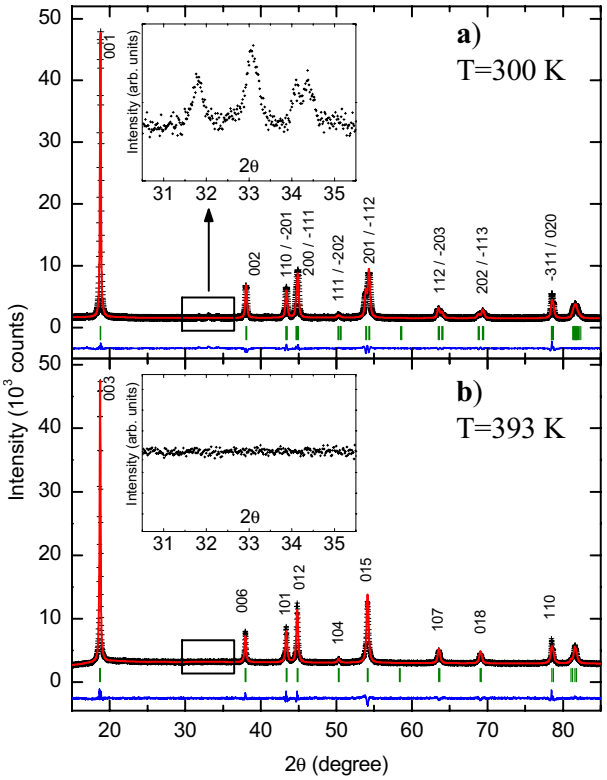

FIG. 1. (Color online) Rietveld refinement of powder XRD pattern of (a) $P'3$-$Na_{0.62}CoO_2$ at 300 K and (b) $P3$-$Na_{0.62}CoO_2$ at 393 K. The observed (crosses), calculated (solid line), and difference (bottom line) profiles as well as Bragg positions (vertical bars) are shown. The 90–120° 2θ range is not displayed for clarity. The insets on both graphs emphasize additional peaks that appear upon cooling and that are not accounted for with the monoclinic cell.

III. STRUCTURE DETERMINATION

X-ray diffraction patterns of $P'3$-$Na_{0.62}CoO_2$ at 300 and 393 K are displayed in Figs. 1(a) and 1(b), respectively. As previously reported,[8] the room temperature XRD pattern of the as-obtained $P'3$-$Na_{0.62}CoO_2$ was accounted for by means of a monoclinic unit cell with space group $C2/m$ and parameters: $a_m=4.8996(6)$ Å, $b_m=2.8263(2)$ Å, $c_m=5.7156(5)$ Å, and $\beta=106.069(6)°$. The insets of Figs. 1(a) and 1(b) focused on the 30–36° 2θ range. Additional weak peaks, each of them representing about 0.6% of the intensity of the strongest (001) peak, are observed in the monoclinic phase and reversibly disappear on heating. Figure 2 displays the XRD patterns recorded from 483 K down to RT for the $32<2\theta<70$ range. Upon cooling, the peak shape significantly changes and the reflections, such as (015), (107), and (018), are split into the monoclinic (201)/(−112), (112)/(−203), and (202)/(−113) doublets, respectively. No indisputable evidence about any possible commensurate or incommensurate ordering of the Na^+ ions within the partially occupied sites was obtained in the present study but, withal,

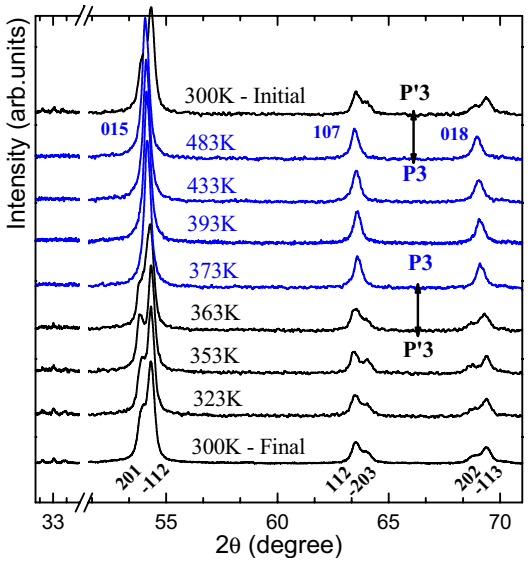

FIG. 2. (Color online) Temperature dependence of XRD patterns of $Na_{0.62}CoO_2$ during cooling for a selected 2θ range, showing that the rhombohedral $P3$ phase becomes stable above 350 K. Reversible vanishing above T_S of additional reflections nearby 33° is attributed to Na^+ ordering within the interlayer.

the reversible vanishing of these peaks above T_S can be considered as manifestations in support of it (right hand side of Fig. 2).

The monoclinic cell parameters and those of the hexagonal cell corresponding to the rhombohedral phase $(\mathbf{a_h}, \mathbf{b_h}, \mathbf{c_h})$ reported by Fouassier *et al.*[6] for $P'3$-$Na_{0.6}CoO_2$ (space group $R3m$) are linked by the following relationship:

$$(\mathbf{a_m}, \mathbf{b_m}, \mathbf{c_m}) = (\mathbf{a_h}, \mathbf{b_h}, \mathbf{c_h}) \begin{bmatrix} 1 & 1 & -1/3 \\ -1 & 1 & 1/3 \\ 0 & 0 & 1/3 \end{bmatrix}. \quad (1)$$

The high temperature data set was successfully fitted by using the space group $R3m$ and the rhombohedral cell proposed by Fouassier *et al.*[6] A Rietveld refinement of the structure at 393 K has been subsequently performed by using these settings. Table I summarizes the structural parameters for $P'3$- and $P3$-$Na_{0.62}CoO_2$ at RT and 393 K, respectively. The atomic positions of cobalt and oxygen atoms have been deduced from Eq. (1): cobalt atoms are distributed in the site (0,0,0); the oxygen atoms occupy two positions, O1 and O2, both in $3a$ site $(0,0,z)$ with $z \sim 0.3901$ and 0.6099, respectively. A different Fourier map clearly shows that sodium atoms are only located in two equivalent positions: the first in $3a$ site $(0,0,z)$ with $z \sim 0.8324$ and the second, also in $3a$ site $(\frac{1}{3}, \frac{2}{3}z)$, with $z \sim 0.8343$. The high temperature stable phase is of $P3$ type, i.e., the structure remains three-layered-like and Na^+ ions are located in trigonal prisms. A representation of both structures is given in Fig. 3.

The primary difference between the high temperature and low temperature forms is that the Na^+ ions reside at a higher symmetry prism for $P3$ structure compared to $P'3$ structure. The Na coordination polyhedra and associated Na-O distances are presented in Fig. 4. In $P'3$, the sodium atoms occupy prismatic sites with Na-O distances ranging from 2.223 to 2.634 Å (Table I). These distances are in good agreement with those generally encountered for this atom. In both structures, the Na-O distances differ whether the oxygens of the CoO_6 octahedra are sharing a face (subscript f) or an edge (subscript e) with NaO_6 prisms. The average Na-O_f distances (2.448 Å in $P'3$ phase and 2.453 Å in $P3$ phase) are larger than the average Na-O_e distances (2.383 Å in $P'3$ phase and 2.430 Å in $P3$ phase). This result can be ascribed to a larger electrostatic repulsion for face-sharing polyhedra (shorter Na-Co distance) than for edge-sharing polyhedra (longer Na-Co distance).

In the monoclinic phase, Na^+ ions are shifted out of the (x,y) center of their prisms, while this is not the case in the rhombohedral phase. When a particular Na site is occupied, the Na-Na distance with its first-nearest-neighbor sites is too small compared to Na^+ diameter to allow simultaneous occupation. The Coulombic repulsion of the Na^+ ion by Na^+ ions occupying second-nearest-neighbor Na sites should therefore dominate Na^+ arrangement within the interslab. Occupying off-centered in-plane positions allow for larger Na-Na sites distances, thereby minimizing the Coulombic repulsion of the Na^+ ions. The distribution of the Na-O distances clearly shows that the Coulombic Na^+-Na^+ repulsion is strong enough to displace the Na^+ ions from the center of their prisms (Table I). Similar electrostatic effects were considered to explain potassium orderings in $K_4Co_7O_{14}$ (Ref. 14) and the off-centered position in $P2$-Na_xCoO_2,[15–17] where two distinct alkaline sites are available. In the two-layered family, the sodium forms many ordered phases with various sodium contents, both commensurate and incommensurate with the underlying CoO_2 hexagonal slabs.[18–20] Direct evidences of structural phase transitions through Na ordering in Na_xCoO_2 upon cooling have also been reported.[21–23] Likewise, the same situation should also be reasonably expected in our system regarding the reversible vanishing of the extra reflections below and above T_S [insets of Figs. 1(a) and 1(b)], and we propose that the vanishing of the Na^+ ordering above T_S is the driving force for the phase transition.

IV. ^{23}Na MAGIC ANGLE SPINNING–NMR SPECTROSCOPY

Powder ^{23}Na MAS-NMR spectra are shown in Fig. 5. The MAS-NMR technique allows averaging both the first-order quadrupolar interactions and nuclear dipolar interactions, which are mainly responsible for the broadening of the NMR lines. At room temperature, the $P3$-$Na_{0.62}CoO_2$ phase exhibits a single shifted signal located around 350 ppm with a clear second-order interaction shape typical of Na^+ ions located in an asymmetric environment. A set of spinning side bands are also observed on both sides of this signal. Note that another signal located around 0 ppm is also observed and assigned to a small amount of diamagnetic sodium impurities in the sample with longer T_1 relaxation time that are not seen by XRD. Its significant decrease as the temperature is raised can be ascribed to the decrease in the population of excited quantum states of the nuclei.[24] At room temperature, an averaging of the cobalt ion charges has been evidenced by

TABLE I. Structural parameters for the monoclinic $P'3$-$Na_{0.62}CoO_2$ at room temperature and the rhombohedral $P3$-$Na_{0.62}CoO_2$ at 393 K.

	$P'3$-$Na_{0.62}CoO_2$ at 300 K	$P3$-$Na_{0.62}CoO_2$ at 393 K	
Space group	$C2/m$ ($Z=2$)	$R3m$ ($Z=3$)	
	Lattice parameters		
a (Å)	4.8995(6)	2.8276(2)	
b (Å)	2.8263(2)	2.8276(2)	
c (Å)	5.7155(5)	16.518(3)	
β (deg)	106.069(6)	106.515(6)[a]	
	Atomic positions		
	Na	Na1	Na2
Sites	8j	3a	3a
(x,y,z)	[0.820(2),0.098(5),0.492(1)]	[0,0,0.8324(3)]	$[\frac{1}{3},\frac{2}{3},0.8343(3)]$
Occ.	0.155	0.31	=Occ. (Na1)
U (Å^2)	0.0076(13)	0.030(3)	=U (Na1)
	Co	Co	
Site	2a	3a	
(x,y,z)	(0,0,0)	(0,0,0)	
Occ.	1	1	
U (Å^2)	0.009(4)	0.008(4)	
	O	O1	O2
Sites	4i	3a	3a
(x,y,z)	[0.3892(6),0,0.1791(4)]	[0,0,0.3901(6)]	[0,0,0.6099(6)]
Occ.	1	1	1
U (Å^2)	0.0076(6)	0.014(4)	=U (O1)
	Selected distances		
Na-O_e (Å)	$1\times2.223(10)$	$3\times2.430(8)$	
	$1\times2.375(12)$		
	$1\times2.551(11)$		
Na-O_f (Å)	$1\times2.318(11)$	$3\times2.453(8)$	
	$1\times2.393(10)$		
	$1\times2.634(12)$		
Co-O (Å)	$2\times1.898(6)$	$6\times1.883(5)$	
	$4\times1.910(3)$		
CoO_2 slab thickness (Å)	1.967	1.876	
NaO_2 interslab thickness (Å)	3.526	3.630	
	Conventional reliability factors		
cR_{wp} (%)	11.1	12.2	
R_{Bragg} (%)	5.71	5.50	
Goodness of fit χ^2	2.99	2.49	

[a]Pseudo-β corresponding to the monoclinic cell for comparison purposes only.

^{59}Co ^{23}Na NMR in several two-layered Na_x and CoO_2 phases.[10,11] Hence, in the $P'3$ and $P3$ phases, the sodium ions are surrounded by equivalent cobalt ions at and above room temperature.

As the temperature increases, the isotropic chemical shift of the Na NMR line is shifted to lower values, denoting Fermi contact mechanism that is in good agreement with the Curie–Weiss paramagnetic behavior of this compound. The temperature elevation also results in a gradual collapse of the second-order quadrupolar line shape and to the emergence of a narrower central resonance. The vanishing of the second-order quadrupolar contribution is expected for a ^{23}Na ion in highly symmetric environment with weak or no electric field gradient (EFG). Upon cooling, exactly opposite effects are observed and the spectra recorded at room temperature at the end of the experiment is similar to the first one (Fig. 5), indicating a good reversibility of the phenomenon.

In the monoclinic $P'3$-$Na_{0.62}CoO_2$ sample at room temperature (Fig. 4), sodium ions occupy crystallographic positions that are shifted out of the center of their prisms. This

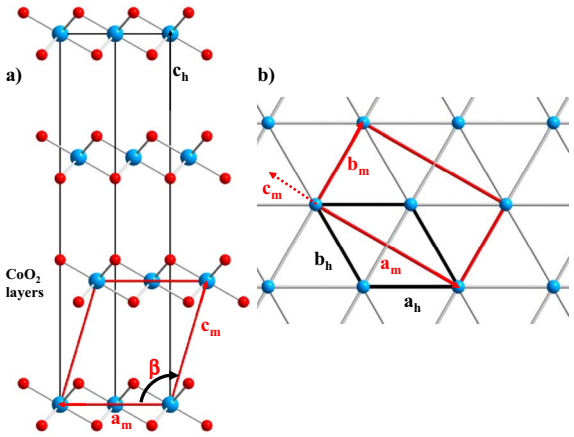

FIG. 3. (Color online) (a) Projection along the b_m axis of the crystal structure relationships between the low temperature monoclinic $P'3$ phase and the high temperature rhombohedral $P3$ phase. Na atoms are not shown for clarity. (b) Projection of the structure along the c_h axis on the Co triangular array ($z=0$), showing the in-plane vectors ($\mathbf{a_h}, \mathbf{b_h}$) and ($\mathbf{a_m}, \mathbf{b_m}$) and projection of the c_m axis (short dashes).

asymmetric oxygen environment of Na is likely to result in strong quadrupolar interactions. Possible Na distribution resulting from the Na and/or vacancy ordering could account for the relatively broad line shape of this second-order quadrupolar signal. As the temperature increases, the gradual disappearance of the second-order line shape and the emergence of a narrower central resonance without quadrupolar second-order shape are resulting from the motion of the sodium cations in the interslab space at the time scale of NMR spectroscopy. Previous ^{23}Na NMR studies on the two-layered $Na_{0.7}CoO_2$ also evidenced Na^+ ion motion above $T=250$ K.[11] Ionic conductance of these lamellar oxides has been known for a long time in the scope of sodium batteries.[1,25] The Na^+ ion's motion pathway between oxygen layers occurring in the tree-layered system is depicted in Fig. 6. Na^+ ions migrate only through the faces of the prisms. The bottleneck radius for sodium in the $P'3$ and $P3$ systems are

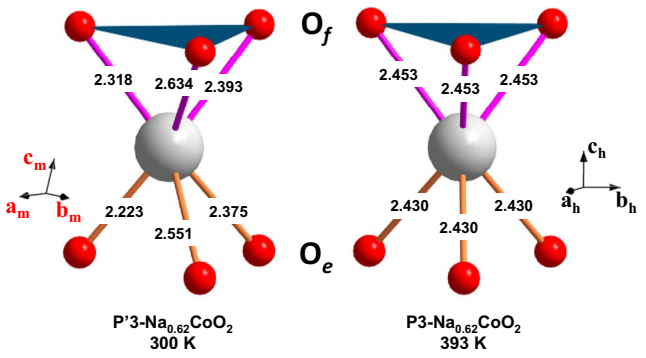

FIG. 4. (Color online) NaO_6 prismatic environments for both $P'3$ and $P3$ phases. The f and e subscripts label oxygen atoms belonging either to a face or to an edge shared by a CoO_6 octahedron with a NaO_6 prism, respectively. The filled triangles show the CoO_6 octahedron faces that are shared with NaO_6 prisms. All distances are in angstroms.

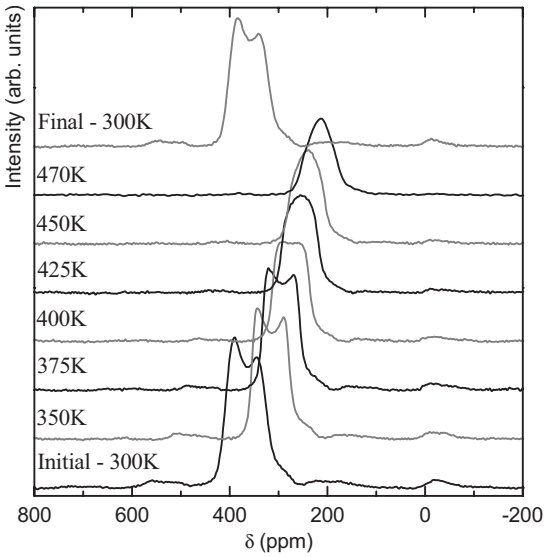

FIG. 5. Temperature dependence of ^{23}Na MAS-NMR spectra for $P'3$-$Na_{0.62}CoO_2$.

calculated to be 0.860 and 0.901 Å, respectively. According to Shannon's radii tables, Na^+ ionic radius in a sixfold polyhedron is estimated to be 1.02 Å. This suggests that Na^+ ions can freely move through this material as there are tunnels available for motion between the oxygen layers, even at room temperature.[26] Two adjacent Na prismatic sites are equivalent in the (ab) plane but opposite along the c direction, which is the main direction of the EFG, resulting in opposite V_{zz} electric field gradient. The mobility of the sodium cations in this phase thus results, by exchange phenomenon, in a cancellation of the V_{zz} contribution and therefore in a signal narrowing and a suppression of the second-order quadrupolar effect. The averaged signal at NMR time scale is therefore similar to the one expected for a single Na^+ ion in a highly symmetric environment. For comparison and as preliminary results, we also studied by ^{23}Na MAS NMR the $P2$-$Na_{0.6}CoO_2$ phase, where the adjacent Na sites are not equivalent regarding the Co environment and the V_{zz} EFG contribution can therefore not be suppressed. In that case, the sodium ions mobility leads to a narrowing of the signal keep-

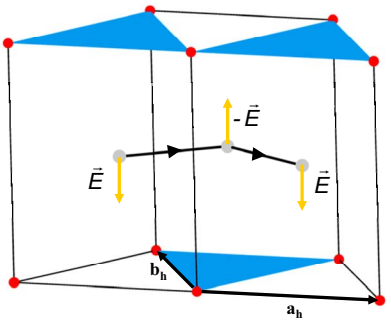

FIG. 6. (Color online) Motion scenario of Na^+ in the interslab. The filled triangles show the CoO_6 octahedron faces that are shared with NaO_6 prisms. The on-site electrical field gradient is schematized by an arrow parallel to the c axis and it is antiparallel for two Na adjacent sites.

ing a clear the 2nd order quadrupolar interaction shape in all the temperature range (300 K to 470 K). These results will be published elsewhere.[27]

The $P'3$-$P3$ phase transition do not correspond to an abrupt change in the ^{23}Na signal, but to a progressive modification from a 2nd order line shape to a symmetric site line shape. This progressive evolution is also true in the $P'3$ phase; therefore the Na mobility increases when temperature increases leading to a progressive cancellation of the V_{zz} main EFG term, as well.

In this picture, the collapse of the second-order quadrupolar line shape and the new resonance observed when the temperature increases mainly originates from fast chemical exchange between sodium sites that is sufficiently fast to average quadrupolar interactions at ^{23}Na MAS-NMR time scale. These observations are in line with the other ^{23}Na MAS-NMR characterizations on zeolites.[28]

V. SPECIFIC HEAT MEASUREMENTS

Figure 7(a) shows the specific heat capacity C_p of the tree-layered $Na_{\sim 0.62}CoO_2$ phase from 1.8 to 400 K. Over the 1.8–270 K temperature range, the data cannot be fitted by using a single Debye model. A better picture of the specific heat was achieved by considering both an electronic contribution and two Debye contributions,[29]

$$C_P(T) = \gamma_{HT}T + 9R\sum_{i=1}^{2} n_i\left(\frac{T}{\theta_i}\right)\int_0^{\theta_i/T}\frac{x^4e^x}{(e^x-1)^2}dx. \qquad (2)$$

The first term $\gamma_{HT}T$ represents the temperature-linear electronic contribution and the second term is the Debye-type contribution (two acoustic modes). $R=8.314$ J/mol K is the molar gas constant, θ_i are the Debye temperatures, and n_i are the number of atoms per mole of $Na_{0.62}CoO_2$ for each Debye mode. The large differences in the bond character between Co-O (covalentlike) and Na-O (ioniclike) and the relatively large mobility of Na^+ ions in the interslab justify the use of two different phonon spectra, each of them being associated with a (θ_i, n_i) couple $(i=1,2)$. A decent agreement with the data set was achieved with $\gamma_{HT}=23.0(1)\times10^{-3}$ J/mol, $\theta_1=291(1)$ K and $\theta_2=855(1)$ K, and n_1 (Na^+ contribution) and n_2 (CoO_2 contribution) being constrained to 0.62 and 3, respectively. $\theta_2(CoO_2) > \theta_1(Na^+)$ is also in good agreement with the highest Co-O bond stiffness compared to Na-O. The Co^{3+}-O bond is very covalent and the covalency increases with the cobalt oxidation state and, as a consequence, a very stiff CoO_2 sublattice is expected for Na_xCoO_2 as x decreases. The large θ_2 value is supported by our studies of the pristinelike $LiCoO_2$ ($\theta_D \sim 800$ K) (Ref. 30) and the available data in the literature for oxides, such as Al_2O_3 ($\theta_D \approx 950$ K),[31] rutile, and anatase TiO_2 ($\theta_D \approx 940$ K),[32,33] GeO_2 ($\theta_D \approx 780$ K),[34] and VO_2 ($\theta_D \approx 760$ K).[35]

At high temperature, a broad peak ranging from 290 to 355 K is observed and its maximum is estimated at around $T_S=350$ K. This transition is attributed to the space rearrangement of Na^+ ions within the network. A similar rearrangement of sodium has been reported in the $P2$-$Na_{0.7}CoO_2$ system, where a large fraction of sodium ions are shifted from a high symmetry $2c$ $(\frac{2}{3},\frac{1}{3},\frac{1}{4})$ site to a lower symmetry $6h$ $(2x,x,\frac{1}{4})$ site.[36] The measured entropy change at the transition is ~0.7 J/mole K. This relatively small value is close to that reported for a $P2$ phase with nearly the same sodium rate.[37] A quantitative discussion of the entropy change value at T_S is beyond the scope of this study as its determination should be based on a more accurate subtraction of background and must take into account the previously mentioned sample radiation losses.

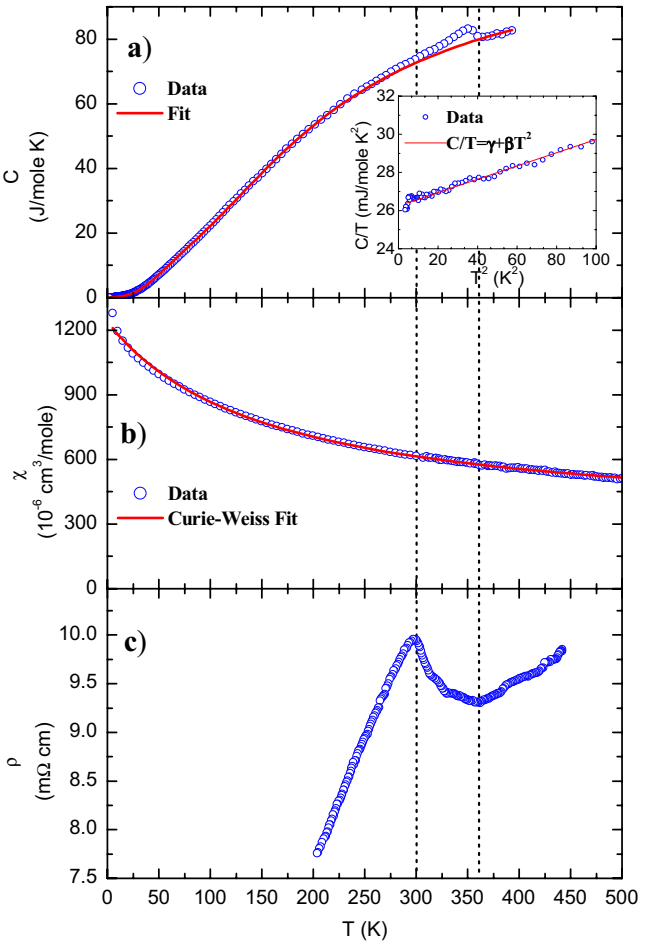

FIG. 7. (Color online) (a) Temperature dependence of the specific heat (open circles), the fit using Eq. (2) (solid line), and the low temperature Debye fit (inset). (b) Temperature dependence of the molar magnetic susceptibility for $Na_{0.62}CoO_2$ (open circles) and the Curie–Weiss fit (solid line). (c) Temperature dependence of the electrical resistivity (open circles). The vertical dotted lines are guide to the eyes and are demarcating the transition domain.

At temperatures below 10 K, the electronic contribution to the specific heat has been calculated by using the Debye model. A linear fit to the data by using $C/T=\gamma+\beta T^2$ equation [inset of Fig. 7(a)] gives $\gamma=26.1(1)\times10^{-3}$ J/mol K^2 and $\beta=3.92(5)\times10^{-5}$ J/mol K^4. The overall θ_D value of 562 K deduced from $\beta=12\pi^4(n_1+n_2)R/(5\theta_D^3)$ is in line with previous estimates[37,38] and is fairly close to the weighted Debye temperature deduced from Eq. (2) and calculated to be 494 K. The γ value is very close to γ_{HT} obtained from Eq. (2) and is about an order of magnitude larger than that of usual metals. The large γ value is consistent with the metal-

liclike character and denotes large electronic correlations. The good agreement between both low and high temperature models indicates that no additional magnetic phenomenon is occurring at low temperature.

VI. MAGNETIC AND ELECTRIC MEASUREMENTS

The magnetic molar susceptibility for $Na_{0.62}CoO_2$ is given in Fig. 7(b). Following previous reports, the data were fitted in the investigated range by using a Curie–Weiss law including a temperature independent term χ: $\chi(T)=\chi_0+C/(T-\theta_p)$, with $\theta_p=-142(3)$ K, $\chi_0=276(5)\times10^{-6}$ cm^3/mol, and $C=0.145(2)$ cm^3 K/mol. A small deviation from the Curie–Weiss law is observed below 30 K, but its origin is unknown.

The negative θ_p value denotes antiferromagnetic interactions between spin carriers. The Curie constant (C) agrees with a ($S=\frac{1}{2}$) spin concentration (or a formal atomic content of low spin Co^{4+}) of 39% ($\mu_{eff}=1.08$ μ_B) in good agreement with the nominal composition. This behavior has been previously ascribed to full spin polarization of itinerant carriers.[39] The coexistence of a large χ_0 with a Curie–Weiss contribution is unexpected. The large positive χ_0 value cannot solely be explained by a second-order orbital (Van Vleck) contribution of low spin Co^{3+} closed $3d$ shells estimated to $\sim150\times10^{-6}$ cm^3/mol and partially balanced by a diamagnetic contribution ($\sim-50\times10^{-6}$ cm^3/mol).[40,41]

In recent studies, partial ($S=\frac{1}{2}$) Co^{4+} hole localization has been suggested, which could account for the antiferromagnetic interactions.[20,42–47] In such a case, localized moments accounting for the Curie–Weiss term could coexist with itinerant carriers accounting for a large χ_0. Clearly, the magnetic properties of these metallic cobaltites for which, depending on the alkali rate x, the magnetic behavior changes from Pauli type ($x<0.5$) to Curie–Weiss type ($x>0.5$) are still not fully understood.[48] In the case of Pauli-type Na_xCoO_2 ($x<0.5$) (Ref. 48) or in potassium homologs ($x=0.6$),[14,49] the Pauli susceptibility value is strongly enhanced by the electronic correlations. No magnetic transition is observed at T_S, which is substantially different from what has been reported in the two-layered system for which weak changes in χ (about 1%) where measured at the temperature of sodium rearrangement.[36,38]

The resistivity at high temperature and upon cooling is reported in Fig. 7(c). A steep departure from the low temperature metallic regime is observed at 297 K, and then, a sharp decrease in ρ occurs up to 360 K, which is followed by another metallic regime. This high temperature feature is associated with the structural transition, which is mainly affecting the Na ion sites and the interslab distance. The latter change can be understood as an increase in the two-dimensional (2D) character with the increase in temperature: the average in-plane Co-Co distances in the $P'3$ and $P3$ phases are almost identical and equal to ~2.8275 Å, whereas the expansion of the c axis leads to a noticeable increase in the NaO_2 interslab distance from 3.526 to 3.630 Å. Simultaneously, the CoO_2 slab thickness decreases from 1.967 to 1.876 Å. In Na_xCoO_2, the c axis increases with decreasing x resulting in a largest compression of the CoO_6 octahedron and an increase in metallicity. The D_{3d} distortion of CoO_6 octahedron lifts the degeneracy of the threefold t_{2g} orbitals into one a_{1g} singlet and one e'_g doublet. Both *ab initio* calculations[50] and experimental works[51,52] provide evidence that the e'_g doublet is stabilized by the D_{3d} distortion. Likewise, this structural change that increases the compression of the CoO_6 octahedra along the c axis may modify the spatial distribution of the a_{1g} and e'_g orbitals and therefore may affect the transport properties.

On the other hand, the sodium distribution in the interslab may also play a role. The ionic contribution of Na^+ ions to the electrical conductivity is much lower than the electronic conductivity and its vanishing through the freezing of the Na^+ ions could not account for the sharp increase in ρ at 297 K upon cooling. Strong correlations between the Na^+ ions and the charge carriers that are ($S=\frac{1}{2}$) holes hopping in a diamagnetic background of Co^{3+} ions are leading to an insulating state at low temperature for $x=\frac{1}{2}$.[48] For $x>0.5$, the effects are expected to remain and the carriers are still influenced by the patterning of Na ions and modulations of Madelung's potential in the interlayers resulting in charge localization.[20,42,46] The freezing of Na^+ atoms could result in the sharp increase in ρ giving rise to a metal-metal transition in our compound. The localization effect is also expected to be enhanced in the three-layered system as each NaO_6 prism is sharing a face with one of the surrounding CoO_6 octahedra. Former reports on the two-layered $P2$ system are further divided into two series: those (in line with this work) characterized by a sharp increase in the resistivity[21,37,53,54] and those (contrasting with this work) showing a sharp drop in resistivity.[36,38] Hysteretic and partially irreversible behavior in the transport properties has been reported in $P2$ phases.[55] Our measurements of the resistivity upon heating (not shown) and cooling show the same anomalies and will be discussed in detail elsewhere. Further work is needed to assess whether charge localization linked to sodium patterning or the increase in the 2D character is the dominant effect in the electronic behavior at the phase transition.

ACKNOWLEDGMENTS

This work was financially supported by the Council of Région Aquitaine, by the Centre National de la Recherche Scientifique (CNRS), and by the French National Research Agency (ANR). M. Ménétrier, E. Bekaert, and M. Pouchard (ICMCB-CNRS) are deeply acknowledged for fruitful discussions. The authors also thank Cathy Denage (ICMCB-CNRS) who provided experimental backup and R. Decourt (ICMCB-CNRS) for technical assistance in transport measurements.

*Corresponding author; maxime.blangero@laposte.net

[1] C. Delmas, J. J. Braconnier, C. Fouassier, and P. Hagenmuller, Solid State Ionics **3-4**, 165 (1981).
[2] J. Molenda, C. Delmas, and P. Hagenmuller, Solid State Ionics **9-10**, 431 (1983).
[3] J. Molenda, C. Delmas, and P. Dordor, Solid State Ionics **12**, 473 (1984).
[4] I. Terasaki, Y. Sasago, and K. Uchinokura, Phys. Rev. B **56**, R12685 (1997).
[5] K. Takada, H. Sakurai, E. T. Muromachi, I. Izumi, R. A. Dilanian, and T. A. Sasaki, Nature (London) **422**, 53 (2004).
[6] C. Fouassier, G. Matejka, J. M. Reau, and P. Hagenmuller, J. Solid State Chem. **6**, 532 (1973).
[7] C. Fouassier, C. Delmas, and P. Hagenmuller, Mater. Res. Bull. **10**, 443 (1975).
[8] Y. Ono, R. Ishikawa, Y. Miyazaki, Y. Ishii, Y. Morii, and T. Kajitani, J. Solid State Chem. **166**, 177 (2002).
[9] L. Viciu, J. W. G. Bos, H. W. Zandbergen, Q. Huang, M. L. Foo, S. Ishiwata, A. P. Ramirez, M. Lee, N. P. Ong, and R. J. Cava, Phys. Rev. B **73**, 174104 (2006).
[10] I. R. Mukhamedshin, H. Alloul, G. Collin, and N. Blanchard, Phys. Rev. Lett. **93**, 167601 (2004).
[11] J. L. Gavilano, D. Rau, B. Pedrini, J. Hinderer, H. R. Ott, S. M. Kazakov, and J. Karpinski, Phys. Rev. B **69**, 100404(R) (2004).
[12] H. M. Rietveld, J. Appl. Crystallogr. **2**, 65 (1969).
[13] J. Rodriguez-Carvajal, Physica B (Amsterdam) **192**, 55 (1993).
[14] M. Blangero, R. Decourt, D. Carlier, G. Ceder, M. Pollet, J. P. Doumerc, J. Darriet, and C. Delmas, Inorg. Chem. **44**, 9299 (2005).
[15] Q. Huang, M. L. Foo, R. A. Pascal, Jr., J. W. Lynn, B. H. Toby, Tao He, H. W. Zandbergen, and R. J. Cava, Phys. Rev. B **70**, 184110 (2004).
[16] L. Viciu, Q. Huang, and R. J. Cava, Phys. Rev. B **73**, 212107 (2006).
[17] J. D. Jorgensen, M. Avdeev, D. G. Hinks, J. C. Burley, and S. Short, Phys. Rev. B **68**, 214517 (2003).
[18] H. W. Zandbergen, M. L. Foo, Q. Xu, V. Kumar, and R. J. Cava, Phys. Rev. B **70**, 024101 (2004).
[19] Y. S. Meng, Y. Hinuma, and G. Ceder, J. Chem. Phys. **128**, 104708 (2008).
[20] M. Roger, D. J. P. Morris, D. A. Tennant, M. J. Gutmann, J. P. Goff, J. U. Hoffmann, R. Feyerherm, E. Dudzik, D. Prabhakaran, A. T. Boothroyd, N. Shannon, B. Lake, and P. P. Deen, Nature (London) **445**, 631 (2007).
[21] Y. Shi, H. C. Yu, C. J. Nie, and J. Q. Li, arXiv:cond-mat/0401052 (unpublished).
[22] H. X. Yang, C. J. Nie, Y. G. Shi, H. C. Yu, S. Ding, Y. L. Liu, D. Wu, N. L. Wang, and J. Q. Li, Solid State Commun. **134**, 403 (2005).
[23] D. Igarashi, Y. Miyazaki, K. Yubuta, and T. Kajitani, Jpn. J. Appl. Phys., Part 1 **46**, 304 (2007).
[24] J. D. Roberts, *Nuclear Magnetic Resonance* (McGraw-Hill, New York, 1959).
[25] C. Delmas, A. Maazaz, C. Fouassier, J. M. Réau, and P. Hagenmuller, Mater. Res. Bull. **14**, 329 (1979).
[26] R. J. Balsys and R. L. Davis, Solid State Ionics **93**, 279 (1996).
[27] D. Carlier, M. Blangero, M. Ménétrier, M. Pollet, J. P. Doumerc, and C. Delmas (unpublished).
[28] K. H. Lim and C. P. Grey, J. Am. Chem. Soc. **122**, 9768 (2000).
[29] N. W. Ashcroft and N. D. Mermin, in *Solid State Physics*, edited by D. G. Crane (Holt, Rinehart and Winston, New York, 1976), Chap. 21, p. 459.
[30] M. Ménétrier, D. Carlier, M. Blangero, and C. Delmas, Electrochem. Solid-State Lett. (to be published).
[31] L. Braginsky, V. Shklover, H. Hofmann, and P. Bowen, Phys. Rev. B **70**, 134201 (2004).
[32] T. R. Sandin and P. H. Keesom, Phys. Rev. **177**, 1370 (1969).
[33] V. Dallacasa, Physica C **437-438**, 57 (2006).
[34] A. Y. Wu and R. J. Sladek, Phys. Rev. B **25**, 5230 (1982).
[35] D. B. McWhan, M. Marezio, J. P. Remeika, and P. D. Dernier, Phys. Rev. B **10**, 490 (1974).
[36] Q. Huang, B. Khaykovich, F. C. Chou, J. H. Cho, J. W. Lynn, and Y. S. Lee, Phys. Rev. B **70**, 134115 (2004).
[37] J. Wooldridge, D. Mc. K. Paul, G. Balakrishnan, and M. R. Lees, J. Phys.: Condens. Matter **17**, 707 (2005).
[38] B. C. Sales, R. Jin, K. A. Affholter, P. Khalifah, G. M. Veith, and D. Mandrus, Phys. Rev. B **70**, 174419 (2004).
[39] Y. Wang, N. S. Rogado, R. J. Cava, and N. P. Ong, Nature (London) **423**, 425 (2003).
[40] G. Lang, J. Bobroff, H. Alloul, P. Mendels, N. Blanchard, and G. Collin, Phys. Rev. B **72**, 094404 (2005).
[41] F. E. Mabbs and D. J. Machin, *Magnetism and Transition Metal Complexes* (Chapman and Hall, London, 1973).
[42] C. A. Marianetti and G. Kotliar, Phys. Rev. Lett. **98**, 176405 (2007).
[43] L. Balicas, Y. J. Jo, G. J. Shu, F. C. Chou, and P. A. Lee, Phys. Rev. Lett. **100**, 126405 (2008).
[44] F. C. Chou, M. W. Chu, G. J. Shu, F. T. Huang, W. W. Pai, H. S. Sheu, T. Imai, F. L. Ning, and P. A. Lee, arXiv:0709.0085 (unpublished); I. R. Mukhamedshin, H. Alloul, G. Collin, and N. Blanchard, arXiv:0703.561 (unpublished); D. J. P. Morris, M. Roger, M. J. Gutmann, J. P. Goff, D. A. Tennant, D. Prabhakaran, A. T. Boothroyd, E. Dudzik, R. Feyerherm, J. U. Hoffmann, and K. Kiefer, arXiv:0803.1312 (unpublished).
[45] G. J. Shu, A. Prodi, S. Y. Chu, Y. S. Lee, H. S. Sheu, and F. C. Chou, Phys. Rev. B **76**, 184115 (2007).
[46] M. H. Julien, C. de Vaulx, H. Mayaffre, C. Berthier, M. Horvatic, V. Simonet, J. Wooldridge, G. Balakrishnan, M. R. Lees, D. P. Chen, C. T. Lin, and P. Lejay, Phys. Rev. Lett. **100**, 096405 (2008).
[47] H. Alloul, I. R. Mukhamedshin, G. Collin, and N. Blanchard, EPL **82**, 17002 (2008).
[48] M. L. Foo, Y. Wang, S. Watauchi, H. W. Zandbergen, T. He, R. J. Cava, and N. P. Ong, Phys. Rev. Lett. **92**, 247001 (2004).
[49] J. Sugiyama, Y. Ikedo, P. L. Russo, H. Nozaki, K. Mukai, D. Andreica, A. Amato, M. Blangero, and C. Delmas, Phys. Rev. B **76**, 104412 (2007).
[50] S. Landron and M. B. Lepetit, Phys. Rev. B **74**, 184507 (2006); **77**, 125106 (2008).
[51] M. Pollet, J. P. Doumerc, E. Guilmeau, D. Grebille, J. F. Fagnard, and R. Cloots, J. Appl. Phys. **101**, 083708 (2007).
[52] D. Qian, L. Wray, D. Hsieh, L. Viciu, R. J. Cava, J. L. Luo, D. Wu, N. L. Wang, and M. Z. Hasan, Phys. Rev. Lett. **97**, 186405 (2006).
[53] M. Mikami, M. Yoshimura, Y. Mori, T. Sasaki, R. Funahashi, and M. Shikano, Jpn. J. Appl. Phys., Part 1 **42**, 7383 (2003).
[54] T. Motohashi, E. Naujalis, R. Ueda, K. Isawa, M. Karppinen, and H. Yamauchi, Appl. Phys. Lett. **79**, 1480 (2001).
[55] T. Ikeda and M. Onoda, J. Phys.: Condens. Matter **18**, 8673 (2006).